Thermochimica Acta 483 (2009) 8–14

Contents lists available at ScienceDirect

Thermochimica Acta

journal homepage: www.elsevier.com/locate/tca

Characterization studies of physicochemical modifications conceded by equimolar-mixed chromia and barium carbonate powders as a function of temperature

L.A. Al-Hajji[a], M.A. Hasan[a], M.I. Zaki[b,*]

[a] Chemistry Department, Faculty of Science, Kuwait University, P.O. Box 5969, Safat 13060, Kuwait
[b] Chemistry Department, Faculty of Science, Minia University, El-Minia 61519, Egypt

ARTICLE INFO

Article history:
Received 19 July 2008
Received in revised form 17 October 2008
Accepted 21 October 2008
Available online 30 October 2008

Keywords:
$BaCO_3$ and Cr_2O_4 powder mixture
Thermochemical interactions
Topochemical interactions
Influence of the surrounding gas atmosphere
Product analysis

ABSTRACT

Occurrence and products of solid/solid interactions in equimolar-mixed $BaCO_3$ and Cr_2O_3 powders were examined isothermally (700–1000 °C) and non-isothermally (25–1200 °C) under different gas atmospheres, employing thermogravimetry, X-ray diffractometry, infrared and Raman spectroscopies, scanning electron microscopy, and energy dispersive X-ray spectroscopy. Irrespective of the gas atmosphere, a non-catalytic decomposition of the barium carbonate commenced at 570 °C, a temperature that is much less than the decomposition temperature (≥970 °C) of separate $BaCO_3$. Characteristics and distribution of the yielding products were found to be quite sensitive to the surrounding gas atmosphere. Under N_2 atmosphere, the interactions were thermochemical in nature, leading eventually to the formation of barium chromite ($BaCr_2O_4$) spinel as the sole detectable product. Under O_2 atmosphere, however, the oxygen molecules contributed oxidatively to the chromite thermal genesis course, thus imposing a topochemical nature to the reaction, leading to formation of $BaCrO_4$, as the major product, and barium chromites ($BaCr_2O_4$ and $Ba_3Cr_2O_6$), as minor products. Proposed reaction pathways and characteristics of products have been presented and discussed.

1. Introduction

Solid-state synthesis is a frequently used method of production of industrially and technologically important materials [1]. Despite the fact that it is more time and energy demanding than other methods, such as mechanochemical [2], sol–gel [3], hydrothermal [4], electrochemical [5] and self-assembly method [6], it is relatively much less sophisticated and, thus, more practical. Moreover, the necessity for high temperatures to trigger the chemical reactivity in reaction mixtures of solids [7] warrants obtaining yields of high thermal and mechanical stabilities; i.e. suitable for heavy-duty applications.

Characterization of thermochemical events involved in solid-state syntheses is a prime demand if a fine control over the product particle properties (size, crystallinity and morphology) would ever be achieved [8]. As a matter of fact, the synthesis of solids of tailored particle properties is largely sought for specific performances [9]. On the other hand, designing of necessary means and ways of control over particle properties requires a full awareness of not only the chemical, but also the physical changes conceded by the reaction mixture throughout the solid-state synthesis course. Topochemical impacts of the surrounding gas atmosphere, i.e. chemical changes influenced by the latter molecules, also worth consideration [8].

Bearing in mind the above considerations, the present investigation was undertaken to characterize physicochemical changes conceded by an equimolar powder mixture of chromia (Cr_2O_3) and barium carbonate ($BaCO_3$) as a function of temperature. The effective temperature range was determined by thermogravimetry, and influence of the surrounding gas atmosphere (oxygen or nitrogen) was probed. Structural modifications of crystalline and non-crystalline domains of the mixture were probed by X-ray diffractometry, and infrared and Raman spectroscopies. Particle morphological modifications were visualized by scanning electron microscopy, whereas the chemical composition was microprobed by energy dispersive X-ray spectroscopy. The principle objective of the investigation was to characterize chemical and physical modifications to be conceded by the reaction mixture to the onset of formation product(s), and to elucidate relationships that may exist between these modifications and nature of the product(s). Probably the most prominent finding of this investigation has been the proven critical dependency of nature of the product(s) on the kind of the surrounding gas atmosphere.

* Corresponding author. Tel.: +20 86 2360833; fax: +20 86 2360833.
E-mail address: mizaki@link.net (M.I. Zaki).

0040-6031/$ – see front matter © 2008 Elsevier B.V. All rights reserved.
doi:10.1016/j.tca.2008.10.014

2. Experimental

2.1. The powder mixture

Powders of chromia (Cr_2O_3) and barium carbonate ($BaCO_3$), 99.5% pure products of Aldrich (USA), were ground to ≤120 mesh, mixed in equimolar quantities by first tumbling the two powders (using a few drops of diethyl ether), and then blending with agate mortar and pestle for 30 min. The resulting powder mixture was found by stereomicroscopy to be at least 75% homogenously mixed, and by preliminary physicochemical characterization (*vide infra*) to have not suffered any detectable mechanochemical activation. It is worth noting that a single patch of the mixture was prepared in a sufficient amount for all tests and analyses performed in the present investigation.

Based on non-isothermal thermogravimetric results (*vide infra*), 5-gm portions of the separate and mixed barium carbonate and chromia powders, placed in pre-cured porcelain crucibles, were calcined at various temperatures (for 3 h in a static atmosphere of air) using electronically controlled Thermolyne 6000 muffle furnace (actual temperature = set temperature ±2 °C). The calcination products were naturally cooled to room temperature (RT) prior to storing over silica gel till further use. For clarity, the uncalcined mixture is denoted below BaCrOx(RT), whereas the calcination temperature applied is used to distinguish calcination products of the mixture. Thus, for example, BaCrOx(800) means the 800 °C calcination product of BaCrOx(RT).

2.2. Thermogravimetry

Thermogravimetry (TG) was carried out, using a model TGA-50H Shimadzu (Japan) automatically recording thermobalance. A small portion (15–20 mg) of test sample was placed in a platinum cell mounted inside the thermobalance, in a dynamic atmosphere of air, oxygen or nitrogen (50 cm^3/min). The mass change was recorded, without correction for possible buoyancy force contributions, on heating up to 1200 °C at 10 °C/min. Data acquisition and handling were facilitated by an on-line workstation (TA-50WS, Shimadzu), and evolved gas analysis by an on-line mass analyzer (a model Thermostar Balzars quadrupole mass analyzer, Switzerland).

2.3. Spectroscopy and microsopy

X-ray powder diffractometry (XRD) was carried out at room and higher temperatures, using a Siemens D5000 diffractometer (Germany) equipped with Ni-filtered Cu K_α radiation (λ = 1.5418 Å, 40 kV and 30 mA), and a high-temperature attachment (Bühler's HDK S1, Germany). The data were acquired stepwise (0.02°/s) in the 2θ range 10–80° with a divergence slit of 1°, and handled with an on-line micro-computer installing standard SEARCH and DIFFRACT AT software (Siemens Corp.) for automatic JCPDS [10] library search and match. Crystallite sizing was carried out implementing the XRD line broadening technique and Scherrer's formula [11]: $D = 0.9\lambda/\sqrt{(B_M^2 - B_S^2)}\cos\theta$, where D is the crystallite size (in Å), B_M and B_S are the width in radians of the diffraction peaks (at half maximum height) of the test sample and a highly crystalline standard sample, respectively, and λ (in Å) is the wavelength of the X-ray beam.

Infrared (IR) and Laser Raman (Ra) spectroscopy were used to characterize crystalline and non-crystalline domains of test samples. IR spectra were taken of KBr-supported test samples (<1 mass%) in the frequency range 4000–400 cm^{-1} (at the resolution of 5.2 cm^{-1}), using a Perkin-Elmer System 2000 FT-IR spectrometer (Germany). Ra spectra were taken of lightly compacted test samples, at 3600–200 cm^{-1} and the resolution of 0.2 cm^{-1}, using a Perkin-Elmer System 2000 FT-Ra spectrometer equipped with a near infrared diode pumped Nd:YAG laser (λ = 1.064 μm and 50–100 mW).

For morphological and elemental microprobing of test samples, a model JSM-6300 Jeol scanning electron microscope (SEM, Japan) equipped with a LINK's exl II Oxford energy dispersive X-ray spectrometer (EDX, U.K.) was employed. The microscope was operated at 20 kV and 100 μA. Test samples, spread in a thin layer over a double adhesive tape on a 10-mm aluminum stub, were sputter-coated with gold prior to examination. EDX data were acquired over 100 s with 2000–3000 X-ray counts per second. The sample preparation was similar to that for SEM examination, except for the gold coating.

3. Results and discussion

3.1. The powder mixture at room temperature

3.1.1. Characteristics of the constituents

X-ray powder diffractograms obtained for separate, uncalcined $BaCO_3$ and Cr_2O_3 powders displayed a number of sharp peaks of high and medium intensities at 2θ = 20–80°. The three strongest peaks are compiled for each material in Table 1. Moreover, Table 1 sets out the average crystallite size derived for each material, using the X-ray line broadening technique [11]. It also shows characteristics of the best matching standard XRD data found for $BaCO_3$ (JCPDS 05-0378) and Cr_2O_3 (JCPDS 38-1479). These results indicate that both of the test powders consist of microcrystallites. Whereas the former powder was found to consist of large crystallites (273 ± 5 Å) of Witherite-like *orthorhombic* structured $BaCO_3$, the latter was found to contain smaller crystallites (164 ± 5 Å) of Eskolaite-like *rhombohedral* structured α-Cr_2O_3.

Observed and reported IR and Ra analysis results of the separate $BaCO_3$ and Cr_2O_3 powders are compared in Table 2. The obvious closeness of the observed band structure and frequencies to those reported for IR and Ra-active vibrations of pure, crys-

Table 1
XRD-derived phase composition and average crystallite size of separate constituents of the test mixture at room temperature.

Constituent	Observed[a]		Reported[b]				Average crystallite size/±5 Å[c]
	d (Å)	*I*/*I*°	*d* (Å)	*I*/*I*°	JCPDS	Phase	
Barium carbonate	3.72	100	3.72	100	05–0378	*Witherite*	273
	3.67	43	3.66	50		$BaCO_3$	
	2.06	33	2.15	30			
Chromium oxide	2.68	97	2.67	100	38–1479	*Eskolaite*	164
	2.49	90	2.48	90		α-Cr_2O_3	
	1.67	100	1.67	90			

[a] The three strongest diffraction peaks.
[b] Found in Ref. [10].
[c] Determined by means of the X-ray line broadening technique [11].

Table 2
Observed and reported IR and Ra results for separate constituents of the test mixture at room temperature.

Constituent	IR				Ra			
	Observed		Reported		Observed		Reported	
	ν (cm^{-1})	Profile[a]	ν (cm^{-1})	[Ref.][b]	$\Delta\nu$ (cm^{-1})	Profile[a]	$\Delta\nu$ (cm^{-1})	[Ref.][b]
$BaCO_3$	2451	w, sp	2499–50	[12,13]	1057	vs, sp	1088–60	[13]
	1750	m, sp	1770–40		688	w, sp	699–80	
	1448	vs, b	1455–35		221	w, sp	233–20	
	1059	w, sp	1065–40					
	856	s, sp	864–34					
	693	m, sp	695–85					
α-Cr_2O_3	649	vs, sp	655–49	[14]	610	s, sp	620–00	[15]
	586	s, sp	580–70		551	vs, sp	560–50	
	444	vw, sp	440–30					
	416	w, sp	420–10					

[a] vw, very weak; w, weak; m, medium; s, strong; vs, very strong; sp, sharp; b, broad.
[b] Source references.

talline $BaCO_3$ [12,13] and Cr_2O_3 [14,15] is quite consistent with the above described XRD results. Apart from the weak IR absorption (at 2451 cm^{-1}) due to νOH vibrations of minority associated surface-OH groups [12,13], all of the observed IR bands (at 1750, 1448, 1059, 856 and 693 cm^{-1}) for $BaCO_3$ are assignable to ν_1–ν_4 C–O vibrations of CO_3^{2-} groups assuming *aragonite*-type site symmetry [12]. Similarly all of the IR bands given rise by the chromia powder (Table 2) are due, solely, to various lattice vibrations of Cr(III)–O bonds organized in α-Cr_2O_3 structure [14]. Consistently, the corresponding Ra bands (Table 2) are assignable solely to Ra-active lattice vibrations of CO_3^{2-} groups (in case of $BaCO_3$) [13] and Cr(III)–O bonds (in case of Cr_2O_3) [15,16].

A further support to the high chemical purity of the separate Cr_2O_3 and $BaCO_3$ powders was provided by EDX microprobing of the particles visualized for these materials in the SEM images displayed in Fig. 1A and B, respectively. The longitudinal, flake-like particles of $BaCO_3$ (Fig. 1B) have given rise to an EDX-determined molecular formula ($Ba_{1.00}C_{1.01}O_{3.02}$) very close to the expected formula ($Ba_{1.0}C_{1.0}O_{3.0}$) for the pure material. Similarly, an EDX-determined molecular formula ($Cr_{1.0}O_{1.51}$) for the smaller and irregularly shaped particles of chromia (Fig. 1A) is very close to that expected ($Cr_1O_{1.5}$) for pure Cr_2O_3. The fact that SEM images shown in Fig. 1A and B reveal larger particles for $BaCO_3$ than Cr_2O_3 is in line with the XRD findings in this regard (see average crystallite sizes given in Table 1).

Thermodynamic data determined (at RT) for pure, crystalline $BaCO_3$ and α-Cr_2O_3 are, respectively, the following: (i) ΔG_f, −1137.7 and −1058.1 kJ/mol; (ii) ΔS_f, 112.1 and 81.2 J/K mol; and (iii) C_p, 85.3 and 120.4 J/K mol [17]. The ΔG_f values of the carbonate and the oxide compounds are rather close, however the lower ΔS_f value of chromia may account for its higher tolerance to mobilization than the barium carbonate.

3.1.2. Influence of mixing

IR spectrum taken of the physical mixture of the carbonate and chromia powders, i.e. BaCrOx(RT), was merely a summation of the absorption bands cited for the separate materials in Table 2. The same is shown (Fig. 1C) to apply to the corresponding SEM micrograph, which helps discerning the much larger particles of the carbonate from the smaller ones of chromia. It also reveals a satisfactory uniform mixing of the reactants' particles. The XRD and Ra results obtained for the physical mixture also served as a kind of summation of results obtained for the separate materials (Tables 1 and 2). These observations confirm that the manual mixing undertaken did not result in sufficient local heating to trigger chemical changes to the mixture composition.

3.2. The reaction mixture at high temperatures

3.2.1. Non-isothermal heating

TG curves obtained on heating at 10 °C/min, in a dynamic atmosphere of air (50 cm^3/min), of the separate powders of $BaCO_3$ (curve a) and Cr_2O_3 (curve b), and their equimolar physical mixture (BaCrOx(RT); curve c) are compared in Fig. 2. It is obvious from the results that $BaCO_3$ is thermally stable to heating up to ca. 970 °C, where it commences suffering detectable mass loss due to thermal decomposition. An earlier differential thermal analysis [18] of $BaCO_3$ revealed occurrence of two mass-invariant, reversible polymorphic transformations at 830 and 940 °C, that is, at the vicinity of its thermal decomposition. In contrast, Cr_2O_3 is shown (Fig. 2, curve b) to remain considerably mass-invariant on heating up to 1200 °C.

The TG curve (c, Fig. 2) obtained for BaCrOx(RT), i.e. the equimolar powder mixture of $BaCO_3$ and Cr_2O_3 indicates mass invariance on heating up to 570 °C, followed, on further heating, by (i) a gradual mass loss (ca. 5.8%) completed near 970 °C and (ii) a subsequent slight, but distinct, mass gain (0.4%) subsiding near 1150 °C. Moreover, the mass loss course is shown to be initially relatively steeper than towards the end.

It is worth noting, that an on-line gas analysis of volatile decomposition products of $BaCO_3$ and BaCrOx(RT) detected nothing but CO_2 molecules, whereas XRD analysis of the solid residues detected BaO (and minority BaO_2) for the separate $BaCO_3$ only. Thus, it is evident that the mass loss conceded by BaCrOx(RT) at 570–970 °C is due to an enhanced decomposition of $BaCO_3$, influenced by Cr_2O_3. The fact that in neither of the calcination products of BaCrOx(RT) at >570 °C (*vide infra*) BaO (or BaO_2) was detected may indicate that the influence of Cr_2O_3 is chemical and not catalytic. Accordingly, the mass loss conceded by BaCrOx(RT) at 570–970 °C is concurrent to a solid-state reaction between components of the powder mixture.

In order to have a deeper insight into the eventual, slight mass gain observed for BaCrOx(RT) at >970 °C (curve c; Fig. 2), two additional TG curves were measured for the physical mixture: a curve was measured in O_2 atmosphere, whereas the other in N_2 atmosphere. The TG curves thus obtained are compared in Fig. 3. The curve (a) obtained in O_2 atmosphere is largely similar to that previously obtained in air (curve c, Fig. 2) in showing the mass loss step to commence also at 570 °C, maximize at 720 °C, slow down detectably as of 780 °C, be followed by the slight mass gain at >970 °C, and result in a net mass loss of 5.4%. In contrast, the curve (b; Fig. 3) obtained in N_2 atmosphere is markedly different. In N_2 atmosphere, the mass loss is shown to commence at the higher temperature of

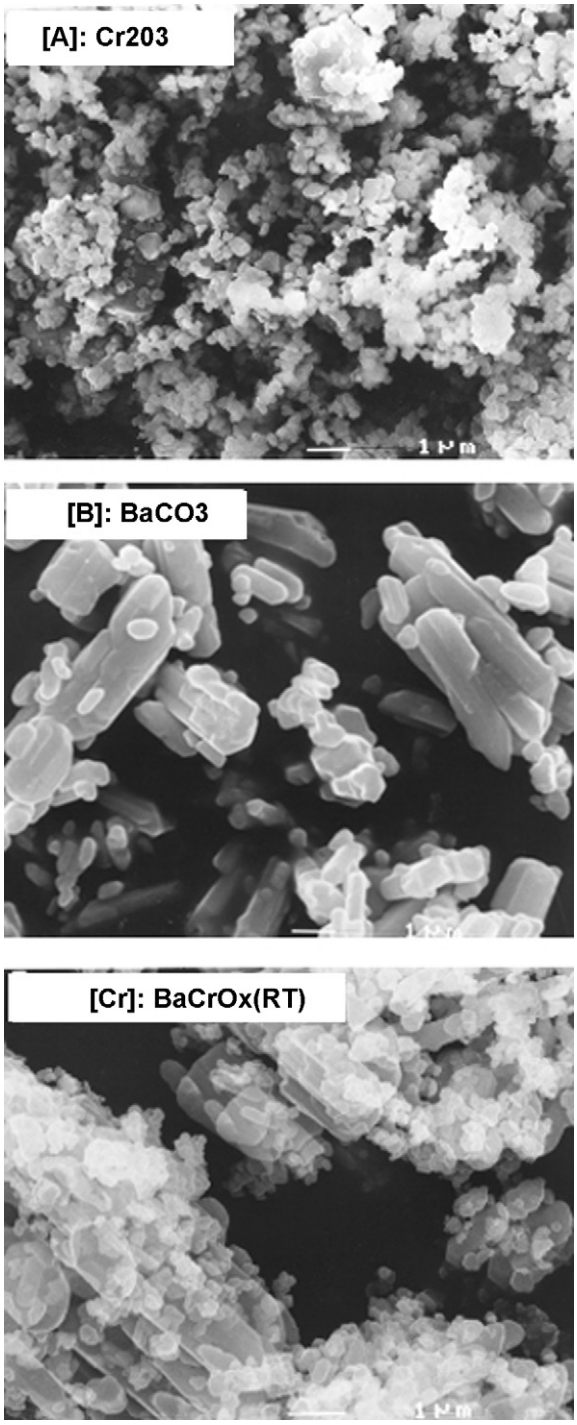

Fig. 1. SEM micrographs obtained for uncalcined, separate (A and B) and equimolar-mixed (C) powders of $BaCO_3$ and Cr_2O_3.

700 °C, maximize at 880 °C, slow down near 940 °C, be followed by an insignificant mass gain (<0.1%), and lead to almost twice as much as the net mass loss observed in air or O_2, viz. 11.6% *versus* 5.4%. It is evident from these results that (i) the solid/solid interaction between $BaCO_3$ and Cr_2O_3 particles, which are responsible for the mass loss observed, is markedly accelerated in the oxidizing atmosphere of O_2 (or air), and (ii) the slow eventual mass loss process is confined to a narrower temperature regime (940–1000 °C) in N_2 atmosphere than that (780–1000 °C) observed in O_2 atmosphere. Furthermore, the much less net mass loss observed in O_2 (or air) than in N_2 atmosphere is due, most likely, to compensation by a considerable, simultaneously occurring mass gain.

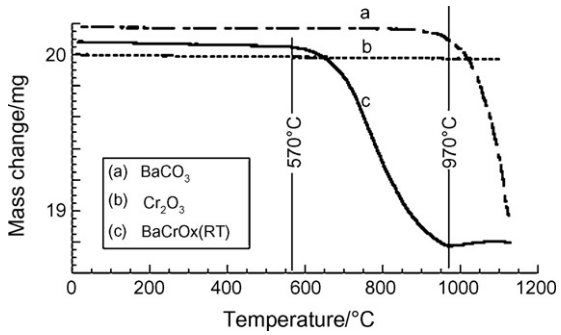

Fig. 2. TG curves obtained on heating (at 10 °C/min and 50 cm³ air/min) of separate (a and b) and equimolar-mixed (c) powders of $BaCO_3$ and Cr_2O_3.

Hence, the results communicated in Fig. 3 reveal that the solid/solid interactions at $BaCO_3/Cr_2O_3$ particle interfaces are quite sensitive to whether the surrounding gas atmosphere is oxidizing (air or O_2) or non-oxidizing (N_2). In N_2 atmosphere, the determined net mass loss (11.6%) is slightly less than that (12.6%) expected for the formation of barium chromite ($BaCr_2O_4$) spinel (the chromium content of which is in the trivalent state (Cr(III)). The slight difference (1%) occurring between these two values may be attributed to the insignificant mass gain observed at ≥1000 °C (curve b, Fig. 3), which might be due to the containment of the nitrogen gas used of trace amounts of O_2, or to the lack of mass measurement correction for possible buoyancy force contributions. Accordingly, solid/solid interactions in N_2 atmosphere are mostly thermochemical in nature.

In O_2 (or air) atmosphere, however, the significant mass gain observed (curve a, Fig. 3) may account for a considerable O_2 uptake and a consequent oxidative contribution to the reaction course; for instance, to the oxidation of Cr(III) into higher-valent chromium, and, hence, formation of chromate species. An example of a similar behaviour is what has been reported in the literature [19] for formation of magnesium chromite ($MgCr_2O_4$) via magnesium chromate ($MgCrO_4$) intermediate upon heating of a powder mixture of MgO and Cr_2O_3 in air. In contrast, formation of cadmium chromate intermediate in the reaction course towards formation of cadmium chromite ($CdCr_2O_4$) in a powder mixture of CdO and Cr_2O_3 (in air) went unnoticed [19]. This fact has been ascribed [19] to the basic character of MgO, which is a requirement not only for stabilization of chromate species, but also for stabilization of metalate species in general [20]. Thus, the known strong basicity of BaO, which has been exploited [20] to justify formation of barium peroxide (BaO_2), can also justify the ability of Ba^{2+} to stabilize high-valent metalate species including chromates.

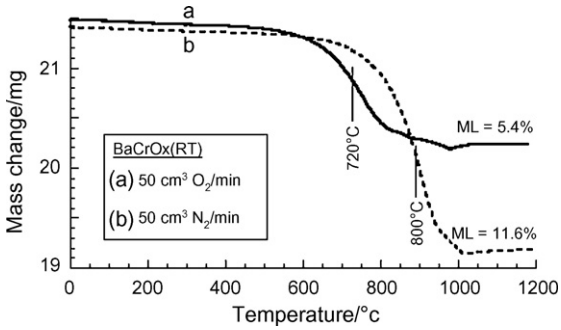

Fig. 3. TG curves obtained on heating (at 10 °C/min and 50 cm³/min) of BaCrOx(RT) in O_2 (curve a) and N_2 (curve b) atmosphere.

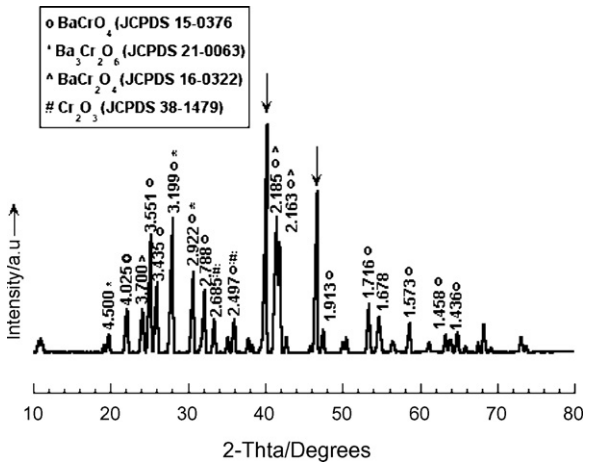

Fig. 4. XRD diffractogram exhibited by the equimolar powder mixture of $BaCO_3$ and Cr_2O_3 following its calcination at 800 °C for 3 h. The diffraction peaks are indicated by the corresponding *d*-spacing values (in Å), whereas those discerned by arrows are due to the Pt/Rh sample holder.

The fact that the separate Cr_2O_3 powder was mass-invariant to heating in the oxidizing atmosphere of air (TG curve b; Fig. 2) may assign the oxygen uptake to freshly genesized species (most likely of BaO) during the very initial reaction steps occurring at the $BaCO_3/Cr_2O_3$ particle interface. In support of such suggestion are several literature reports [e.g., 21–23] confirming that the oxidation of Cr(III)–O species is facilitated on the surface rather than in the bulk, and as they crystallize into the compact α-chromia phase the high-valent Cr–O species, thus obtained, are destabilized and deoxygenated back to the initial Cr(III)–O species.

3.2.2. Isothermal heating

HT-XRD powder diffractograms were obtained upon in-situ heating up to 1000 °C (in air) of BaCrOx(RT), allowing for a 10-min isothermal heating at each set temperature. These diffractograms were sought to determine the on-set temperature of the chemical reactivity, within the XRD error margin, leading to a crystalline product(s) in the reaction mixture. Results obtained revealed that it was not until the temperature reached 700 °C that detectable diffraction peaks other than those diagnostic of the reactants emerged. On further increase of the temperature, those emerging peaks intensified, and additional peaks appeared. Due to the short duration of heating (10 min) these emerging diffraction peaks were generally weaker than those of the reactants.

Accordingly, calcination of BaCrOx(RT) was carried out ex-situ at various temperatures in the range from 700 to 1000 °C for a longer period of time (3 h). A typical example of the X-ray powder diffractograms of the calcination products is that shown for the product at 800 °C (BaCrOx(800)) in Fig. 4. As indicated in the figure, most of the major diffraction peaks displayed are assignable to a *Hashemite*-like $BaCrO_4$ (JCPDS 15-0376). Rest of the peaks may account for minority phases of $Ba_3Cr_2O_6$ (JCPDS 21-0063) and $BaCr_2O_4$ spinel (JCPDS 16-0322) products, as well as a small amount of unreacted Cr_2O_3. None of the peaks displayed could be unequivocally assigned to unreacted $BaCO_3$. Similar XRD results were obtained for the powder mixture following calcination at the lower temperature of 700 °C, except for the detection of trace amounts of a compound assuming the composition of $Ba_3(CrO_4)_2$ that is filed in JCPDS 24–159. The fact that this latter product is a Cr(V)-compound may be considered indicative of its being as an oxidation product and, probably, a precursor for further oxidation to the Cr(VI)-compound ($BaCrO_4$). Its absence to XRD of BaCrOx(800) (Fig. 4) may be thought of as being due to enhancement of its oxidative transformation to the chromate compound.

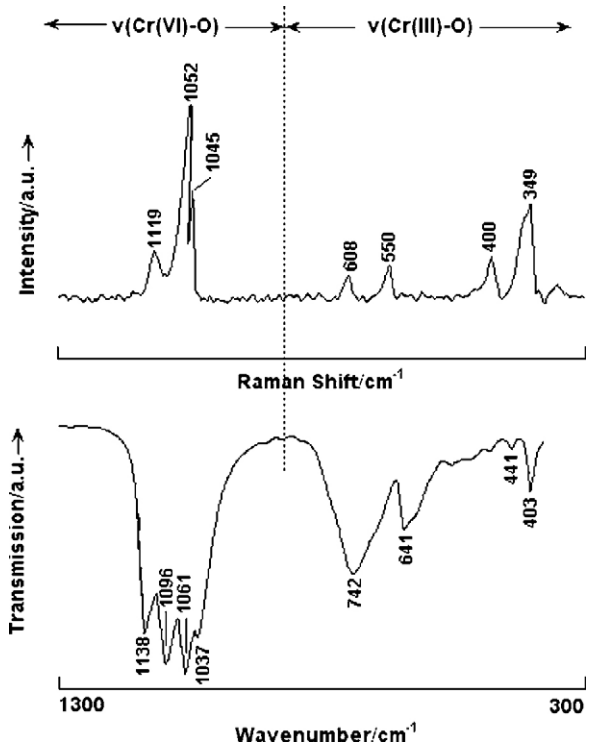

Fig. 5. IR and Ra spectra taken of the 800 °C calcination product of the equimolar powder mixture of $BaCO_3$ and Cr_2O_3.

It is worth noting, that 800 °C calcination products of separate $BaCO_3$ and Cr_2O_3 powders gave rise to almost the same XRD, IR and Ra results as before calcination (Tables 1 and 2). This observation confirms persistence of the separate reactants to the high-temperature heating in air, and, hence, attributes the formation of the XRD-detected $BaCrO_4$, as a major product, and $Ba_3Cr_2O_6$ and $BaCr_2O_4$, as minor products, to solid-state interactions involving the reactant particles and oxygen gas molecules. Moreover, the fact that the chemical composition and mass of the separate Cr_2O_3 phase remain invariant to the high-temperature treatment in air can, indeed, exclude the α-chromia particles from being the primary target of the oxidative action of the oxygen molecules.

IR and Ra spectra taken from BaCrOx(800), Fig. 5, are quite consistent with the corresponding XRD results, Fig. 4. This is in the sense that both spectra display peaks assignable, solely, to bond vibrations of Cr(VI)–O species at >1000 cm^{-1}, and Cr(III)–O at <1000 cm^{-1} [12,14,16,21]. These results may, moreover, confirm the absence of crystalline products other than the XRD-detected ones; i.e. $BaCrO_4$, $Ba_3Cr_2O_6$ and $BaCr_2O_4$.

SEM images obtained for the 800 °C calcination products of separate and equimolar-mixed powders of $CaCO_3$ and Cr_2O_3 are compared in Fig. 6. Accordingly, particle morphologies of the separate $BaCO_3$ and Cr_2O_3 powders (Fig. 6A and B) are shown to remain similar to those observed before calcination (Fig. 1A and B). In contrast, the SEM of BaCrOx(800), Fig. 6C, visualizes a departure from the initial particle morphologies of the uncalcined mixture (Fig. 1C). After calcination, the longitudinal particles of $BaCO_3$ (Fig. 1B) are hardly discernable in the product's image (Fig. 6C). Instead, two different particle morphologies are exhibited: (i) considerably large particles of well defined crystal habit and facets (particles (a); Fig. 6C and the inset magnified image), and (ii) agglomerates of much smaller particles of irregular contours (par-

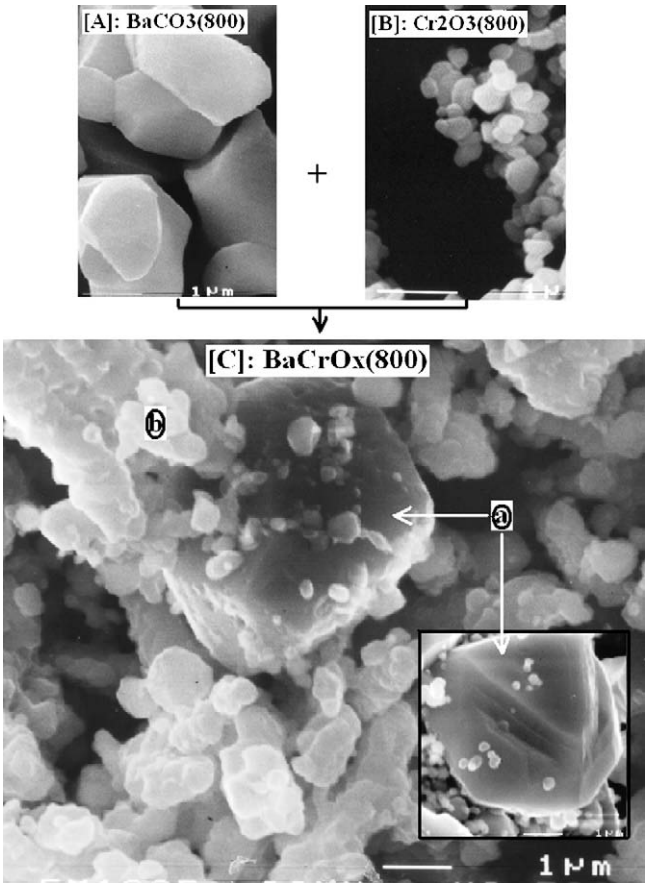

Fig. 6. SEM micrographs obtained for the separate (A and B) and equimolar-mixed (C) powders of $BaCO_3$ and Cr_2O_3 following their calcination at 800 °C for 3 h. The EDX microprobing results of the (a)- and (b)-labeled locations of the micrograph (C) are set out in Table 3.

ticles (b); Fig. 6C). Molecular stoichiometry calculations based on EDX analysis results of these particles (a and b, Fig. 6C) resulted in the data compiled in Table 3. Accordingly, the chemical composition derived for the large particles (a), $Ba_{1.0}Cr_{1.0}O_{4.1}$ (Table 3), is very close to that expected for the $BaCrO_4$ product. On the other hand, the composition derived for the small-particle agglomerates (b), $Ba_{0.01}Cr_{1.0}O_{7.5}$, may account for a chromium and oxygen rich composite of mixed Cr(III)–Cr(VI)–oxygen compounds, or of highly polymeric chromate. Probably, particles (b) are of precursor/intermediate compounds to the major $BaCrO_4$ product.

The product distribution characterized in thermally treated equimolar-mixed powders of $BaCO_3$ and Cr_2O_3 may help envisaging different scenarios of interaction events involving the reactant particles, depending on the surrounding gas atmosphere. In the non-oxidizing atmosphere of N_2 gas molecules, these interactions

Table 3
EDX-analysis results for the locations marked "a" and "b" in Fig. 6C for BaCrOx(800).

Location	Element	Line	Proportion[a]		Derived composition
			(%)	(atomic)	
"a"	O	K-ser	25.79	1.611	$Ba_{1.0}Cr_{1.0}O_{4.1}$
	Cr	K-alpha	20.40	0.392	
	Ba	K-ser	53.81	0.392	
"b"	O	K-ser	69.24	4.328	$Ba_{0.01}Cr_{1.0}O_{7.5}$
	Cr	K-alpha	29.85	0.574	
	Ba	K-ser	0.920	0.007	

[a] Normalized data.

are shown (Fig. 3) to go straight on to the formation of $BaCr_2O_4$ spinel compound:

$$BaCO_{3(s)} + Cr_2O_{3(s)} \rightarrow BaCr_2O_{4(s)} + CO_{2(g)}\uparrow; \quad (1)$$

where, s = solid and g = gas.

The absence of detectable, separate phases of BaO or BaO_2 at any stage throughout the reaction course might be considered suggestive of a unidirectional migration of Cr(III)–O species towards the reaction front. The thermodynamic data presented and discussed in Section 3.1 may lend a support to such a suggestion. In the oxidizing atmosphere of O_2 gas molecules, the formation of $BaCr_2O_4$ spinel seems to have been considerably hampered by a competitive oxidation reaction of Cr(III) into higher valencies by activated oxygen molecules. The oxygen activation is most likely facilitated by the known tolerance of freshly genesized barium oxide species to the following redox cycle: $2BaO_{(s)} + O_{2(g)} = 2BaO_{2(s)}$ [22]. Peroxide species are reactive oxidants [22]. Hence, formation of the XRD-detected oxidation product $Ba_3(CrO_4)_2$, which declares oxidation of Cr(III) into Cr(V) species, may be represented by the following conceptual equation:

$$4BaCO_{3(s)} + Cr_2O_{3(s)} + 1.5O_{2(g)} \rightarrow Ba_3(CrO_4)_{2(s)} + BaO_{2(s)} + 4CO_{2(g)}\uparrow . \quad (2)$$

In fact, the Cr(V)-compound is detectable, in minor proportions, at ≤700 °C only, whereas BaO_2 escapes detection through out the reaction course. Hence, both compounds are, most likely, intermediates to subsequent products, but BaO_2 seems to be used up at a faster rate than $Ba_3(CrO_4)_2$.

The barium monochromate ($BaCrO_4$) and chromite ($BaCr_2O_4$), which are XRD-detected as major and minor products, respectively, at ≥700 °C may be thought to form concurrently via the following further reaction of the BaCr(V)Ox and BaO_2 intermediate species with chromia species:

$$Ba_3(CrO_4)_{2(s)} + 2Cr_2O_{3(s)} + BaO_{2(s)} \rightarrow 2BaCrO_{4(s)} + 2BaCr_2O_{4(s)}. \quad (3)$$

Summation of Eqs. (2) and (3) results in the following overall Eq. (4), which depicts the topochemical nature of the solid-state reaction involving particles of $BaCO_3$ and Cr_2O_3, and oxygen gas molecules:

$$4BaCO_{3(s)} + 3Cr_2O_{3(s)} + 1.5O_{2(g)} \rightarrow 2BaCrO_{4(s)} + 2BaCr_2O_{4(s)} + 4CO_{2(g)}\uparrow . \quad (4)$$

The fact that XRD-detected relatively larger proportions of $BaCrO_4$ than $BaCr_2O_4$ in the high-temperature (800–1000 °C) calcination products of BaCrOx(RT) may be ascribed to differences in the crystallization rates of the two compounds, or to occurrence of the following alternative reaction course:

$$2BaCrO_{4(s)} + Cr_2O_{3(s)} \rightarrow BaCr_2O_{7(s)} + BaCr_2O_{4(s)} \quad (5)$$

$$3BaCr_2O_{7(s)} + Cr_2O_{3(s)} \rightarrow 2BaCr_3O_{10(s)} + BaCr_2O_{4(s)} \quad (6)$$

In this alternative reaction course, the chromite spinel is thought to form as a decomposition product of the monochromate compound. However due to the high thermal stability of the monochromate, its decomposition, often, occurs via a slow deoxygenating polymerization into polychromates [23,24]. Ammonium polychromates as high as $(NH_4)_2Cr_3O_{10}$ and $(NH_4)_2Cr_4O_{13}$ have been successfully synthesized and characterized [24].

As a matter of fact, the eventual mass loss determined for the reaction in oxygen atmosphere (5.4%, Fig. 3) cannot be met neither exactly nor approximately by a postulated overall reaction unless it is leading to formation of a polychromate; for

instance,

$$2BaCO_{3(s)} + 5Cr_2O_{3(s)} + 7.5O_{2(g)} \rightarrow 2BaCr_5O_{16(s)} + 2CO_{2(g)} \ldots (ML = 6.3\%)$$

4. Conclusion

The above presented and discussed results may help drawing the following conclusions as to the solid/solid interactions occurring at particle interfaces in powder mixtures of $BaCO_3$ and Cr_2O_3:

1. A non-catalytic, thermochemical decomposition of $BaCO_3$ particles is triggered by interactions at solid/solid interfaces with Cr_2O_3 particles, at a much lower temperature (570 °C) than the decomposition temperature (≥ 970 °C) of a separate barium carbonate in the atmosphere of air.
2. In the non-oxidizing atmosphere of N_2 gas molecules, the reaction goes straight on to the formation of barium chromite, $BaCr_2O_4$, as the sole detectable crystalline product at 700–1000 °C.
3. In the oxidizing atmosphere of O_2 gas molecules, the oxygen is uptaken presumably by chemisorption at freshly genesized interfaces of BaO/Cr(III)–O. Consequently, topochemical interactions at BaO_2/Cr(III)–O thus generated may lead to oxidation of the Cr(III)–O species into higher-valent chromium and formation of $Ba_3(CrO_4)_2$ intermediate compound at ≤700 °C, whose further reaction with Cr_2O_3 at higher temperatures results in the formation of barium monochromate, $BaCrO_4$.
4. Formation of barium chromite, $BaCr_2O_4$, in the oxygen atmosphere most probably follows further interaction of the barium monochromate and Cr_2O_3 to the onset of formation of barium polychromate and chromite.

Acknowledgements

The financial support facilitated by the college of post-graduate studies, and the excellent technical support found at Science Analytical Facility (*SAF*) and Electron Microscopy Unit (*EMU*) of the faculty of Science of Kuwait University are highly appreciated.

References

[1] C.N.R. Rao, in: V.V. Boldyrev (Ed.), Reactivity of Solids: Past, Present and Future, Blackwell Science, London, 1996, pp. 237–252.
[2] V.V. Zyryanov, Inorg. Mater. 36 (2000) 54.
[3] K.M.S. Khalil, M.I. Zaki, Powder Technol. 120 (2001) 256.
[4] B. Xie, Y. Wu, Y. Jiang, F. Li, J. Wu, S. Yuan, Y. Qian, J. Cryst. Growth 235 (2002) 283.
[5] P. Krtil, M. Yoshimura, J. Solid State Electrochim. 2 (1998) 321.
[6] S. Kwan, F. Kim, J. Akana, P. Yang, Chem. Commun. 5 (2001) 447.
[7] C.H. Bamford, C.F.H. Tipper (Eds.), Comprehensive Chemical Kinetics: Reactions in the Solid State, 22, Elsiever, Amsterdam, 1980.
[8] H. Schmalzried, Chemical Kinetics of solids, VCH-Verlag, Weinheim, 1995.
[9] V.V. Boldyrev, in: V.V. Boldyrev (Ed.), Reactivity of Solids: Past, Present and Future, Blackwell Science, London, 1996, pp. 267–286.
[10] Standard diffraction data JCPDS files, International Center for Diffraction Data, Newton Square, PA 19073-3273, USA.
[11] H.P. Klug, L.E. Alexander, X-ray Diffraction Procedures for Polycrystalline and Amorphous Materials, 2nd ed., J. Wiley & Sons, New York, 1974, pp. 618–706.
[12] J.A. Gadsden, Infrared Spectra of Minerals and Related Inorganic Compounds, Butterworths, London, 1975.
[13] F.A. Miller, G.L. Carlson, F.F. Bently, W.H. Jones, Spectrochim. Acta 16 (1960) 135.
[14] R. Marchall, S.S. Mitra, P.J. Gielisse, J.N. Plendi, C. Mansur, J. Chem. Phys. 43 (1965 2893).
[15] K. Nakamoto, Infrared and Raman Spectra of Inorganic and Coordination Compounds, 5th ed., J. Wiley & Sons, Chichester, 1977, pp. 180–184.
[16] J.M. Stencel, Raman Spectroscopy for Catalysts, Van Norstrand Reinhold, New York, 1990.
[17] I. Barin, Thermochemical Data of Pure Substances, Part I & II, VCH-Verlag, Weinheim, 1993.
[18] M.I. Zaki, R.B. Fahim, Powder Technol. 33 (1982) 161.
[19] H. Charcosset, P. Turlier, Y. Trambouze, J. Chim. Phys. 1249 (1964) 1257.
[20] R.B. Fahim, M.I. Zaki, G.A.H. Mekhemer, Powder Technol. 33 (1982) 33.
[21] J.A. Campell, Spectrochim. Acta 21 (1965) 851.
[22] J.C. Bailar, H.J. Emeleus, R. Nyholm (Eds.), Comprehensive Inorganic Chemistry, vol. 1, Pergamon Press, Oxford, 1973, pp. 591–664.
[23] T.V. Rode, Oxygen Compounds of Chromium Catalysts, Izd. Akad. Nauk SSSR, Moscow, 1962.
[24] T.V. Rode, in: J.P. Redfern (Ed.), Thermal Analysis, Macmillan, London, 1965, pp. 122–123.